molecules

MDPI

Article

Adsorption Characteristics of Gas Molecules Adsorbed on Graphene Doped with Mn: A First Principle Study

Tingyue Xie [1,2], Ping Wang [2], Cuifeng Tian [2], Guozheng Zhao [1], Jianfeng Jia [1], Chaozheng He [3], Chenxu Zhao [3,*] and Haishun Wu [1,*]

[1] Key Laboratory of Magnetic Molecules and Magnetic Information Materials of Ministry of Education, School of Chemistry and Materials Science, Shanxi Normal University, Taiyuan 030006, China; tingyuexie@126.com (T.X.); zhaoguozheng@sxnu.edu.cn (G.Z.); jiajf@dns.sxnu.edu.cn (J.J.)
[2] School of Physical and Electronics Science, Shanxi Datong University, Datong 037009, China; wangping061226@aliyun.com (P.W.); cftian_050@sxdtdx.edu.cn (C.T.)
[3] Institute of Environmental and Energy Catalysis, School of Materials Science and Chemical Engineering, Xi'an Technological University, Xi'an 710021, China; hecz2019@xatu.edu.cn
* Correspondence: zhaochenxu@xatu.edu.cn (C.Z.); wuhs@sxnu.edu.cn (H.W.)

Abstract: Herein, the adsorption characteristics of graphene substrates modified through a combined single manganese atom with a vacancy or four nitrogen to CH_2O, H_2S and HCN, are thoroughly investigated via the density functional theory (DFT) method. The adsorption structural, electronic structures, magnetic properties and adsorption energies of the adsorption system have been completely analyzed. It is found that the adsorption activity of a single vacancy graphene-embedded Mn atom (MnSV-GN) is the largest in the three graphene supports. The adsorption energies have a good correlation with the integrated projected crystal overlap Hamilton population (-IpCOHP) and Fermi softness. The rising height of the Mn atom and Fermi softness could well describe the adsorption activity of the Mn-modified graphene catalyst. Moreover, the projected crystal overlap Hamilton population (-pCOHP) curves were studied and they can be used as the descriptors of the magnetic field. These results can provide guidance for the development and design of graphene-based single-atom catalysts, especially for the support effect.

Keywords: density functional theory (DFT); electronic structure; charge transfer; -pCOHP; Fermi softness

check for updates

Citation: Xie, T.; Wang, P.; Tian, C.; Zhao, G.; Jia, J.; He, C.; Zhao, C.; Wu, H. Adsorption Characteristics of Gas Molecules Adsorbed on Graphene Doped with Mn: A First Principle Study. *Molecules* **2022**, *27*, 2315. https://doi.org/10.3390/molecules27072315

Academic Editor: T. Jean Daou

Received: 3 March 2022
Accepted: 30 March 2022
Published: 2 April 2022

Publisher's Note: MDPI stays neutral with regard to jurisdictional claims in published maps and institutional affiliations.

Copyright: © 2022 by the authors. Licensee MDPI, Basel, Switzerland. This article is an open access article distributed under the terms and conditions of the Creative Commons Attribution (CC BY) license (https://creativecommons.org/licenses/by/4.0/).

1. Introduction

Hydrogen sulfide (H_2S) is a toxic and corrosive gas, which can be easily found in raw natural gas, the by-product gas flow of petroleum processing plants (due to the presence of sulfur in crude oil), and the waste gas flow from petrochemical plants, the paper industry, and coal gasification furnaces [1]. Titanium-modified carbonaceous materials can effectively extract hydrogen from hydrogen sulfide [2]. Formaldehyde (CH_2O) is widely used in building and decoration materials, and is the most common indoor air pollutant [3]. Boron nitride nanosheets with N vacancy defects are treated as a promising candidate for the detection of CH_2O in pioneering works [4]. Moreover, hydrogen cyanide (HCN), a kind of cyanide, is a very powerful colorless poison. It can inhibit the oxygen consumption of human tissues and is highly lethal to humans and animals [5]. The reactivity and electronic sensitivity of original and structure-modified BC_2N nanotubes (BC_2NNT) for the capture of HCN molecules were investigated [6]. These studies show that it is necessary to find effective adsorbents for these high reactive gas molecules.

Graphene-based devices, including photovoltaics [7], spintronic devices [8], gas sensors [9] and graphene-based composite materials [10], have attracted wide attention in the field of two-dimensional materials owing to their excellent electronic, mechanical, photonic and thermal characters [11–22]. In addition, graphene has been proved to be a promising carrier for single-atom catalysts (SACs) due to its orbital hybridization and charge transfer

between the substrate and single atoms [23,24]. The single Co active site on the graphene base embodies good electrochemical stability and high electrocatalytic activity for the reduction of triiodide [25]. Gold atom embedded in the single hole of graphene has low cost and high catalytic activity for CO oxidation [26]. High catalytic activity and selectivity have become vital aims to be achieved in the areas of chemicals and energy.

Introducing appropriate dopants into graphene materials can significantly improve the chemical activity and stability of the materials. In recent years, theoretical studies have been carried out on the adsorption of NO_2, NH_3, SO_3, H_2S, HCN and other gas molecules on graphene (GN) doped with metal atoms (TM). These results show that these catalysts have high stability and play a potential role in the field of electronic devices and gas sensors [27–33]. MnN_4-GN also has excellent selectivity and sensitivity for CO detection [34]. Al-doped graphene can enhance high sensitivity for detecting CH_2O molecules [35]. From the above studies, it can be inferred that it is necessary to synthesize precisely modified SACs with a single atom tightly fixed on the support.

It is necessary to consider the selection of a single TM atom catalyst on the support in order to fill this gap. Recently, Robertson et al. found that the Fe-doped graphene has good selectivity of a magnetic and non-magnetic state and the structure of the complex is also stable [36]. Graphene with pyridine nitrogen defects (FeN_4-GN and MnN_4-GN) have been successfully synthesized and their electronic properties and formation energies have been changed [37,38]. As an efficient catalyst for CO oxidation, FeN_4-GN features a stable configuration, low cost and high activity [39]. The catalytic activity of MnN_4-GN has also been focused on for ORR application [40]. The types of structural defects in graphene include single vacancies (SV) and divacancy (DV), which can dramatically regulate their charge and reactivity properties [41,42]. In addition, the doping of transition metal (TM) atoms can solve the chemical inertness issue of intrinsic graphene, and transition metal atoms can be treated as highly active centers for molecular adsorption. Therefore, we investigated three types of graphene-based catalysts with single-atom manganese. They were expressed as MnX-GN (X = SV, DV or N_4) systems, respectively. In this work, it was necessary to investigate the electronic structure, geometric stability, adsorption energy, charge transfer, spin polarization and magnetic properties of CH_2O, H_2S and HCN gases on MnX-GN in detail by DFT calculation. We further investigated the influence factors of adsorption energy by plotting the predicted density of states (PDOS), -pCOHP and the electron density difference. Finally, the correlation between the adsorption activity and the graphene-based support was further understood by analyzing the electronic properties and Fermi softness of MnX-GN catalysts. This investigation provided here shows that non noble metal-doped graphene supports for the synthesis of high activity SACs are of great significance.

2. Computational Details and Methods

All spin polarized density functional theory (DFT) calculations and the projector augmented wave (PAW) pseudopotentials method are performed within the Vienna ab initio simulation package (VASP) [43–45]. The generalized gradient approximation (GGA) with the Perdew–Burke–Ernzerhof (PBE) functional is used to describe the exchange and correlation potential [44]. The van der Waals (vdW) interaction between gas and surface of MnX-GN catalysts plays a key role in the adsorption; thus, gas adsorption on metal-doped graphene has been successfully studied with the vdW correction [46,47]. Therefore, the interaction of vdW is considered with DFT-3 in our work [48]. We use a hexagonal supercell ($4 \times 4 \times 1$) with periodic boundary condition as the infinite graphene sheet and the supercell vacuum spacing is set to 15 Å, which is sufficiently large to obtain reliable results [49]. The C–C bond length calculated after optimization is 1.426 Å, which agrees well with previous reports [50,51]. All molecule structures can be visualized with the VESTA 3 program [52]. The crystal orbital Hamilton population (COHP) is used to analyze the interaction between molecules and surfaces [53–55].

A plane wave energy cutoff was chosen to be 500 eV, and the width of Gaussian broadening scheme is 0.05 eV occupation of electron level. In order to improve calculation accuracy and save time simultaneously, a k-point grid with $7 \times 7 \times 1$ as the center is used to sample the Brillouin region for structural optimization. When the energy change is less than 10 meV/atom, the k-point grid test is finished. The k-point mesh of $15 \times 15 \times 1$ is used to calculate the density of state (DOS). In the geometric optimization process, the position relaxation of all atoms is calculated by conjugate gradient method until the maximum force is smaller than 0.02 eV/Å. The total energy convergence accuracy is 10^{-5} eV for the electronic self-consistent steps. The cubic cells of 15 Å × 15 Å × 15 Å are used to simulate the energy of isolated atoms (or gas molecules). The atomic charge and electron transfer in the adsorption system were evaluated by Bader charge analysis [56].

In order to easily describe the energy and the electron density difference in this paper, the binding energy (E_b) between the adsorbed atoms Mn and X-GN is defined as $E_b = E_{MnX\text{-}GN} - E_{X\text{-}GN} - E_{Mn}$, where E_{Mn}, $E_{MnX\text{-}GN}$ and $E_{X\text{-}GN}$ are the energy of Mn atom in vacuum, the total energy of MnX-GN and the energy of X-GN (X-GN stand for graphene of SV, DV or N_4), respectively. The adsorption energy (E_{ad}) of gas molecules on MnX-GN is calculated using the expression as $E_{ad} = E_{gas\text{-}Mn/GN} - E_{Mn/GN} - E_{gas}$, where $E_{gas\text{-}Mn/GN}$ indicates the total energies of gases/MnX-GN complex, $E_{Mn/GN}$ denotes the total energy of MnX-GN, E_{gas} is the energy of gas molecule. A larger negative value of E_b and E_{ads} demonstrates a stronger interaction. The expression defines the electron density difference as $\Delta\rho = \rho_{gas\text{-}Mn/GN} - \rho_{Mn/GN} - \rho_{gas}$, where $\rho_{Mn/GN}$ represents the electron density of MnX-GN, $\rho_{gas\text{-}Mn/GN}$ is the electron density of gases/MnX-GN and ρ_{gas} is the electron density of gas.

3. Results and Discussion

3.1. Model of MnX-GN

The stable geometric configurations of MnSV-GN, MnDV-GN and MnN_4-GN are shown in Figure 1. Through the calculation, the absorption height, charge transfer, binding energy and the total magnetic moments are summarized in Table S1. For MnX-GN substrates, three adsorption sites are considered, including single vacancy, divacancy and four nitrogen decorated defects. The binding energies of embedded Mn are calculated with the values of −6.12, −5.86 and −6.61 eV, respectively. The corresponding adsorption heights are 1.40, 0.70 and 0.03 Å, respectively. Estimated from the Bader charge analysis, the Mn atoms are all positively charged with 0.88, 1.06 and 1.28 |e|, respectively, which agrees with previous works [49,57]. For MnX-GN systems, the cohesive energy of Mn bulk (−2.92 eV per atom) is smaller than the binding energy of Mn [58], indicating that the Mn atom can be well scattered in graphite bases. In other words, this kind of substrate can prohibit the aggregation of manganese atoms from clustering. Therefore, our designed systems possess great geometric stability.

The electronic properties, including charge transfer and magnetic moment, of MnSV-GN, MnDV-GN and MnN_4-GN are shown in Table S1. The negative value of the transferred charge from Mn to the substrate indicates that Mn acts as the donor of electrons and graphene acts as the acceptor. The total magnetic moments of doped Mn are 3.00, 2.94 and 3.05 μ_B, respectively, which is consistent with the data in pioneering works [34,57]. As shown in the PDOS of Figure S1, high localized spin density is observed on TM and coordinated nitrogen (carbon) atoms.

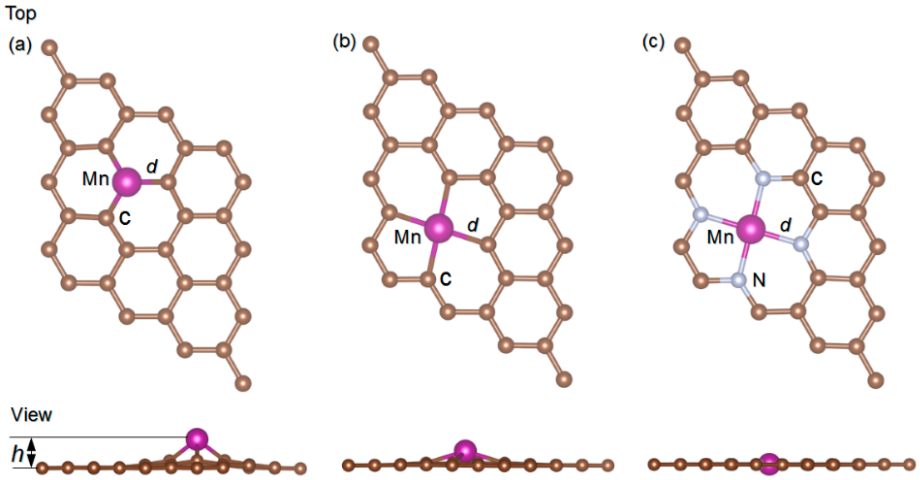

Figure 1. Optimized structures of (**a**) MnSV-GN, (**b**) MnDV-GN and (**c**) MnN_4-GN, the bond lengths (d, Å), adsorption height of Mn atom (h, Å).

3.2. Adsorption Structure, Adsorption Energy

The adsorption structures of CH_2O, H_2S and HCN on three MnX-GN catalysts were optimized and the most stable structures for each gas were found. The optimized configurations and parameters of adsorption systems are shown in Figures 1 and 2.

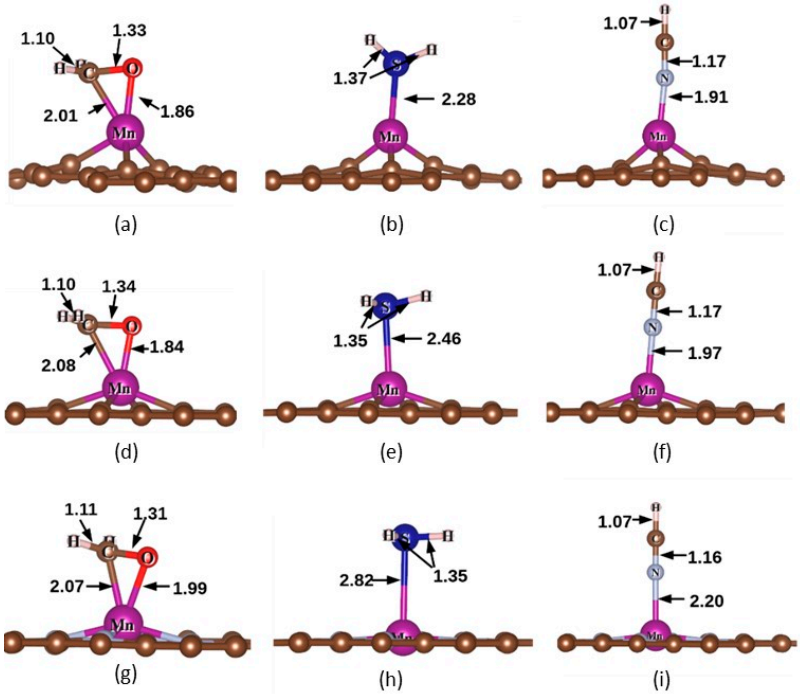

Figure 2. The optimized structures of (**a**) CH_2O/MnSV-GN, (**b**) H_2S/MnSV-GN, (**c**) HCN/MnSV-GN, (**e**) CH_2O/MnDV-GN, (**f**) H_2S/MnDV-GN, (**g**) HCN/MnDV-GN, (**h**) CH_2O/MnN_4-GN, (**i**) H_2S/MnN_4-GN and (**j**) HCN/ MnN_4-GN. The selected bond distance is expressed in angstroms.

In order to investigate the influence of gas adsorption on MnX-GN catalysts, adsorption energies of three gas/MnX-GN catalysts are calculated, as listed in Table S2. The adsorption energies (E_{ad}) of CH_2O on AlN and InN monolayers were −1.04 and −1.05 eV, respectively [59], which is much lower than that on MnSV-GN (−1.86 eV, see Table S2), indicating that the adsorption activity of MnSV-GN is higher compared to AlN and InN monolayers. The E_{ad} of H_2S on the MnSV-GN surface was −0.83 eV (see Table S2), which was similar to the NiSV-GN system (−0.70 eV) [60]. The E_{ad} of HCN on CoSV-GN is −0.30 eV [61], which

is obviously smaller than that on MnSV-GN (−1.11 eV in Table S2). The E_{ad} of HCN on MnSV-GN (−0.60 eV) [29] is obviously smaller than the results in this work (−1.11 eV in Table S2). Therefore, it is shown that the adsorption activity of Mn is higher than that of Co and Ni systems. In addition, the adsorption energies of gases on the MnSV-GN catalyst were higher than that on MnDV-GN and MnN_4-GN, corresponding to a higher reactivity. The adsorption energies of gases on MnSV-GN range from −0.83 to −1.86 eV, indicating a chemical adsorption (>0.5 eV) behavior (see Table S2). Moreover, the chemisorbed behavior can also be reflected in Figure 2, where the molecules can form chemical bonds with Mn atoms in the substrates.

After the gas adsorbing on the MnX-GN catalysts, the uplift heights of Mn atoms are summarized in Table S2. Gas molecules can lift Mn atoms higher during the adsorption process. The adsorption configurations of the same gas on three MnX-GN catalysts are similar, but the uplift heights of Mn atoms are significantly different. The order of the uplift heights is as follows: MnN_4-GN > MnDV-GN > MnSV-GN, which agrees with the pioneering works [31].

Moreover, a completed linear fitting between the adsorption energies and the value of the integrated projected COHP (-IpCOHP) is obtained as depicted in Figure 3a–c. Notably, the correlation coefficients are all greater than 0.85, indicating that there is a significant positive correlation between -IpCOHP values and adsorption energies. Therefore, the -IpCOHP values can be used as the descriptor of adsorption strength. The -IpCOHP values of the three gases on MnDV-GN and MnN_4-GN are lower than those on MnSV-GN, indicating that the two catalysts have lower activity compared to MnSV-GN.

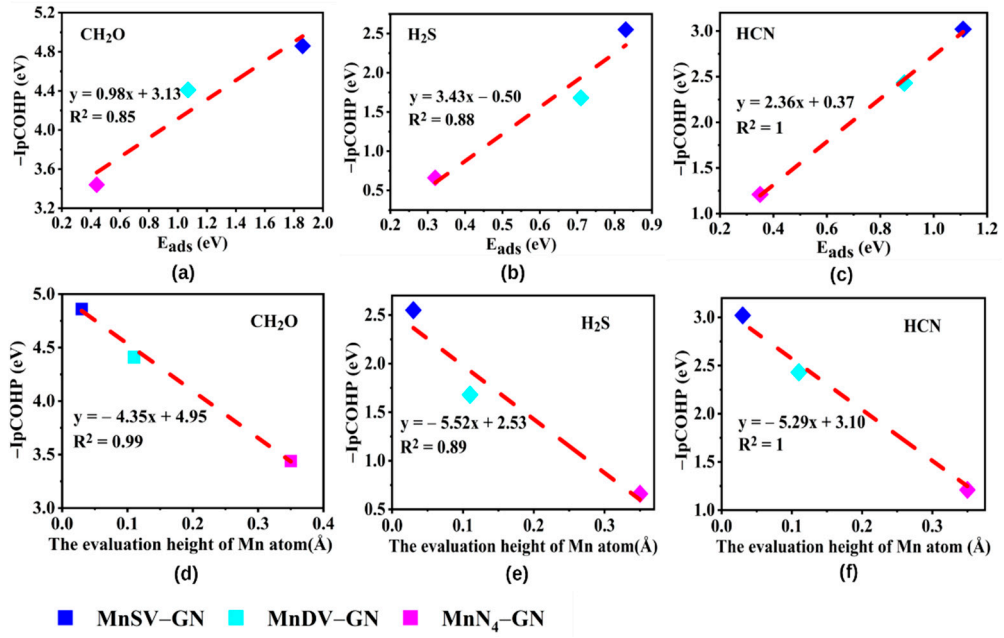

Figure 3. The -IpCOHP values of gases as a function of adsorption energies of (**a**) CH_2O, (**b**) H_2S, and (**c**) HCN and Mn atomic heights of (**d**) CH_2O, (**e**) H_2S, and (**f**) HCN.

In order to clarify the correlation among the adsorption energies, height and -IpCOHP values of the three gases on MnX-GN, the average height differences of the three gases on MnX-GN are calculated with the values as 0.03 Å, 0.11 Å and 0.35 Å, respectively. From Figure 3d–f, it can be concluded that the -IpCOHP values decrease as the height difference of Mn atoms increase, and it is remarkable that the correlation coefficients between the -IpCOHP values of the three gases and the height of the hump are all greater than 0.9, indicating that there is a significant negative correlation between the -IpCOHP values and the height of the hump. Therefore, the height difference of the Mn atom can be used as the activity descriptor of the adsorption system.

3.3. Electronic Structure and Magnetic Properties

The type of gas adsorption will affect the electronic structure distribution of the substrate, including chemical and physical adsorption. We have also investigated the Bader charge and the charge density difference between the gas molecules and MnX-GN (Figure S2 and Table S3), showing that the doped metal atom can enhance the interaction between the reactant and substrate. For example, the charge density difference between the reactive CH_2O gas and MnX-GN was analyzed, as listed in Figure S2a,e,j. It was found that the distribution of electrons is mainly concentrated near CH_2O molecules, indicating the electron acceptor nature of CH_2O. Similar changes are found in Figure S2c,g,j for HCN adsorption. However, in Figure S2b,f,i, the positive charge is mainly distributed around the H_2S molecule, indicating the electron donor nature, which is similar to the case of FeDV-GN [24]. Moreover, the calculation results of Bader charge are consistent with those of electron density difference. From these results, it can be inferred that the redistribution of charge is mainly caused by the adsorption of gas molecules.

In order to clarify the magnetic properties of gas-adsorbed MnSV-GN, the magnetic moment was analyzed in the process of gas adsorption. By comparing the magnetic moments in Tables S1 and S3, we found that the change in magnetic strength for the gas/MnSV-GN system is the biggest (from 3.00 to 1.00 μ_B). To further discuss the cause of different magnetic properties of the gas/MnX-GN system, the projected crystal overlap Hamilton population (-pCOHP) curves between the gas and the surface were analyzed. The results show that the Mn-C bond in the MnSV-GN structure exhibits anti-bonding features around the Fermi level, which implies a potential electronic instability, as illustrated in Figure S3a. When the three gases were adsorbed on the MnSV-GN (Figure S3b–d), the interaction between the Mn and C atoms exhibited significant differences from that in Figure S3a. The change in magnetic properties for the gas/MnN_4-GN system is smallest (from 3.05 to 2.90 μ_B). Moreover, the three gases-adsorbed MnN_4-GN systems can also be analyzed by -pCOHP curves (see Figure S4). As shown in Figure S4b–d, the curves of -pCOHP between Mn and N atoms exhibit nearly no change after gas adsorption. This may indicate that the adsorption of gas molecules has nearly no effect on the magnetic behavior of the substrates. The three gases adsorbed on the MnDV-GN system can also be analyzed by the -pCOHP curve (see Figure S5). There exists a significant difference between the situations in Figure S5a,b on the interaction between the Mn atoms and C atoms. However, there is nearly no difference between Figure S5c,d. The -pCOHP curve analysis is consistent with the magnetic moments in Table S3. These illustrated that the magnetic property of MnX-GN can be adjusted by gas adsorption. From another point of view, the MnSV-GN catalyst has a stronger activity.

It is observed that the distribution of spin density underwent more remarkable changes between the gas and MnSV-GN support, as depicted in Figure S6a–c. The up spin is dominant on the Mn atom in MnSV-GN, which is opposite for the carbon atom adjacent to Mn. In the case of the three gas-adsorbed MnN4-GN, the spin density is depicted in Figure S6h–j, respectively. The spin electron distribution (the yellow area) of CH_2O/MnDV-GN composite is mainly concentrated on the O atoms of CH_2O molecules and Mn atoms (see Figure S6e). For H_2S- and HCN-adsorbed MnDV-GN systems (see Figure S6f,g), the spin density of H_2S is strongly localized around the Mn atom, and the adsorption of HCN leads to the local polarization of the whole system. In general, the results of the spin density analysis are consistent with the magnetic moment calculation.

3.4. Electronic Structure–Reactivity Analysis

In order to explore the relationship between the adsorption effect and the electric structure of MnX-GN catalysts, Fermi softness analyses were performed. Based on the chemical reaction theory, the entire frontier electron band on the solid surface participates in the reaction [62,63], and the electronic states near the Fermi level contribute more to the bonding interaction. Hence, both weight functions ($w(E)$) and density of states ($g(E)$) can determine the reactivity of the solid surface. This can quantify the contribution of

each electronic state to surface bonding [62]. The Fermi softness (S_F) is defined by the weighted sum of the reactivity contributions, which is the reactivity index of the solid surface. Namely, S_F can be expressed by the formula (Equation (1)):

$$S_F = \int_{-\infty}^{+\infty} g(E)w(E)dE \quad (1)$$

where $g(E)$ can be assigned from the total density of states, $w(E)$ can be assigned from the derivative of the Fermi–Dirac function, $-f'_{\mathrm{T}}\,(E - E_F)$. The $-f'_{\mathrm{T}}\,(E - E_F)$ can be expressed by the formula (Equation (2)):

$$-f'_{\mathrm{T}}\,(E - E_F) = \frac{1}{kT} \cdot \frac{1}{(e^{(E-E_F)/kT} + 1)(e^{(E_F-E)/kT} + 1)} \quad (2)$$

where T is the parametric temperature, k is Boltzmann's constant and E_F is the Fermi level. The $w(E)$ distribution is affected by the value of kT, so the Fermi softness is significantly affected by the value of kT. Fermi softness is considered to have a quantitative relationship with surface reactivity [62]. Gao et al. extended Fermi softness and applied it to a single atom catalyst system [31]. When kT is 1.35 eV, one has also calculated the relationship of S_F and adsorption energy between the four Fe/GS and Hg^0 [64]. Therefore, it is necessary to select a suitable kT value to analyze the activity of the catalyst by Fermi softness.

In order to clarify the effect of kT on Fermi softness, the Fermi softness of MnX-GN was calculated at different values of kT (Figure 4a). In Figure 4a, the S_F of MnX-GN adsorbents gradually increase and then decrease with the increased kT. Based on the fact that Fermi softness and adsorption energy have a very strong correlation at this appropriate kT temperature [10], we have also used the maximum correlation coefficient (R^2) to find the appropriate kT value. In Figure 4b, the magenta, red and blue dotted lines represent the kT values of the CH_2O, H_2S and HCN, respectively, corresponding to the maximum correlation coefficients. The R^2 curves of CH_2O, H_2S and HCN have the largest peaks at kT = 2.8, 1.7 and 1.9 eV, respectively. When kT is 2.8 eV, R^2 has the maximum value of 0.94. At this temperature, the Fermi softness of MnX-GN is around 7.8~8.2 eV. When kT is 1.7 and 1.9 eV, the correlation coefficient (R^2) curves of H_2S and HCN are all 1. At 1.7 and 1.9 eV temperature, the Fermi softness of MnX-GN for H_2S and HCN is around 6.4~7.0 and 6.8~7.3 eV, respectively. Therefore, the selected kT value is very important for the Fermi softness analysis due to the fact that Fermi softness correlates intimately with the value of kT.

In order to further verify the relationship between the adsorption energy and Fermi softness, the curve of the adsorption energies of CH_2O, H_2S and HCN can be plotted as a function of Fermi softness (in Figure 5). From Figure 5, the maximum value of R^2 under kT = 2.8 (1.7, 1.9 eV) is 0.93 (1, 1) and there is a significant negative correlation between Fermi softness and adsorption energy. The higher the adsorption energy is, the larger the Fermi softness. Moreover, Fermi softness can be used as an efficient descriptor for the adsorption analysis of single-atom Mn-doped catalysts.

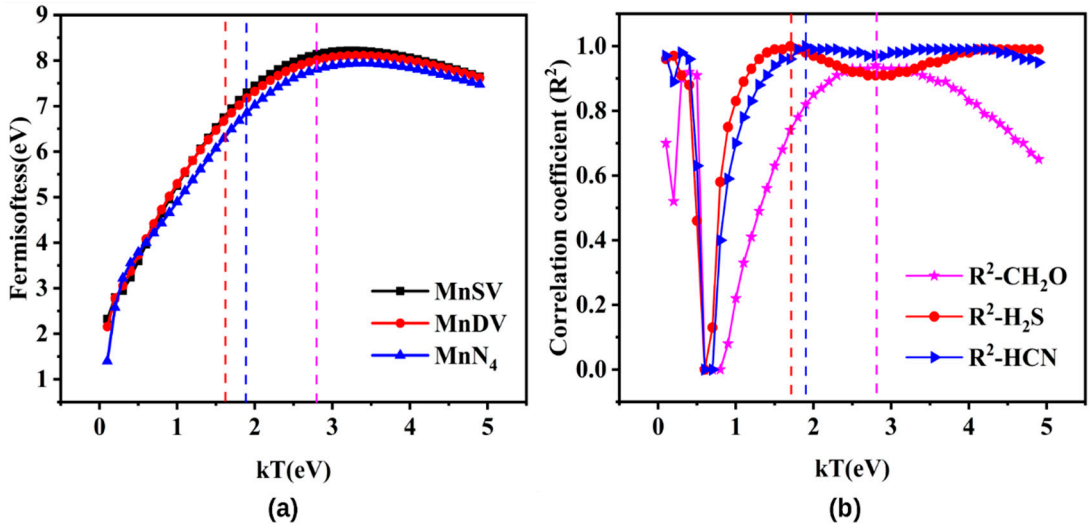

Figure 4. The effect of *kT* on (**a**) Fermi softness of MnX-GN and (**b**) the square correlation coefficient.

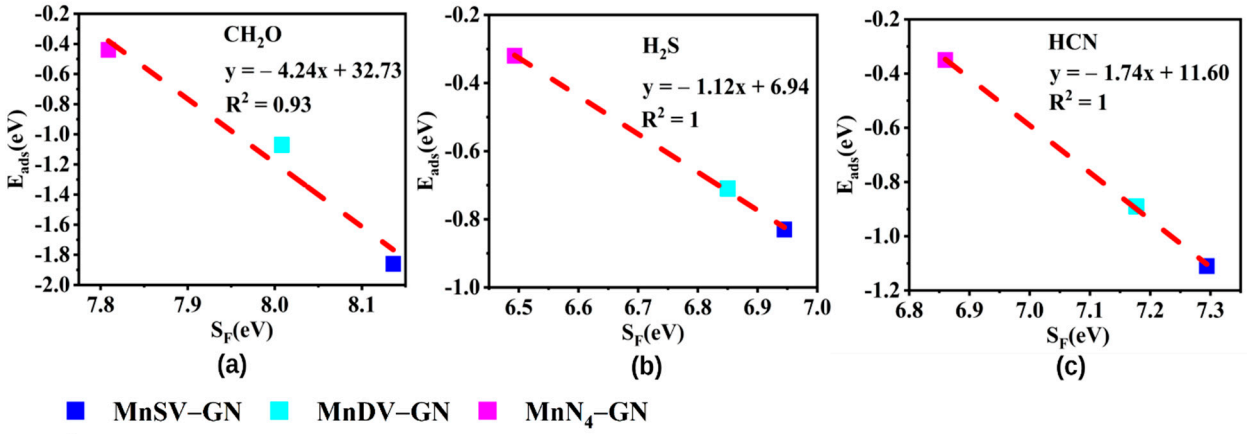

Figure 5. The adsorption energies of (**a**) CH_2O, (**b**) H_2S and (**c**) HCN as a function of Fermi softness.

4. Conclusions

In summary, by using the density functional theory, the adsorption properties, including adsorption energy, adsorption geometry, electronic structure and spin distribution, of CH_2O, H_2S and HCN are investigated on MnSV-GN substrates with different defects. The order of the uplift height of Mn atoms is as follows: MnN_4-GN > MnDV-GN > MnSV-GN. The electronic structure of the graphene support determines the adsorption characteristics of CH_2O, H_2S and HCN. Among the adsorption energies of the three gases on MnX-GN bases, MnSV-GN is the largest, indicating that the adsorption activity of MnSV-GN is higher than that of MnDV-GN and MnN_4-GN.

The adsorption energy of the gas/MnX-GN system is linearly related to the uplift height, IpCOHP values and Fermi softness. The variety in anti-bonding and bonding characteristics on every side of the Fermi level in the magnetic -pCOHP curves can be used as the magnetic field strength descriptor of the adsorption system. The adsorbed activity results are consistent with those analyzed by Fermi softness. Properties such as Fermi softness, the uplift height and -IpCOHP can be used as important indicators of adsorption activity when we theoretically design new graphene support materials. Therefore, we hope that the Mn-doped graphene of our research can become an effective resource and provide viable materials for improving the design of graphene-based support.

Supplementary Materials: The following supporting information can be downloaded at: https://www.mdpi.com/article/10.3390/molecules27072315/s1. Table S1: The absorption height (h, Å) of Mn atoms; Average distance between the dopant and its neighboring C or N atoms (d, Å); Amount of charge transfer (Δq, e, the acquisition or loss of electrons is indicated by the "+" or "−") from Mn atom to supports; Binding energies (E_b, eV); The total magnetic moments (M, μ_B), Table S2: The uplift height of Mn atoms; The -IpCOHP values of various atomic interactions; The adsorption energies (E_{ad}) of gas molecules on MnSV-GN, MnDV-GN and MnN_4-GN; Total -IpCOHP values of Mn-C and Mn-O for CH_2O; -IpCOHP values of Mn-S for H_2S; -IpCOHP values of Mn-N for HCN, Table S3: The charge changes of adsorbed gases (Δq); Total magnetic moment (M) after gas adsorption; Change of magnetic moment (ΔM) before and after gas adsorption (Δq, the acquisition or loss of electrons is indicated by the "+" or "−"), Figure S1: Projected density of states (PDOS) of (**a**) MnSV-GN, (**b**) MnDV-GN and (**c**) MnN_4-GN. The arrow up and arrow down indicate the spin up and spin down states, respectively, Figure S2: Charge density difference ($\Delta\rho = \rho_{A+B} - \rho_A - \rho_B$) of (**a**) CH_2O/MnSV-GN, (**b**) H_2S/MnSV-GN, (**c**) HCN/MnSV-GN, (**e**) CH_2O/MnDV-GN, (**f**) H_2S/MnDV-GN, (**g**) HCN/MnDV-GN, (**h**) CH_2O/MnN_4-GN, (**i**) H_2S/ MnN_4-GN and (**j**) HCN/ MnN_4-GN. The accumulation and depletion of electrons are represented by the yellow and cyan regions, respectively, isosurface value: 0.003e $Å^{-3}$, Figure S3: -pCOHP curves for the dopant Mn and its neighboring C interactions (**a**) MnSV-GN (**b**) CH_2O/MnSV-GN, (**c**) H_2S/MnSV-GN and (**d**) HCN/MnSV-GN in spin-polarized (magnetic) calculations. α-spin (spin up) and β-spin (spin down) is indicated by blue color and red color, Figure S4: -pCOHP curves for the dopant Mn and its neighboring N interactions (**a**) MnN_4-GN (**b**) CH_2O/MnN_4-GN, (**c**) H_2S/MnN_4-GN and (**d**) HCN/MnN_4-GN in magnetic (spin-polarized) calculations. α-spin in blue color and β-spin in red color in the magnetic calculations, Figure S5: -pCOHP curves for the dopant Mn and its neighboring C interactions (**a**) MnDV-GN (**b**) CH_2O/MnDV-GN, (**c**) H_2S/MnDV-GN and (**d**) HCN/MnDV-GN in magnetic (spin-polarized) calculations. α-spin in blue color and β-spin in red color in the magnetic calculations, Figure S6: The spin density of (**a**) CH_2O/MnSV-GN, (**b**) H_2S/MnSV-GN, (**c**) HCN/MnSV-GN, (**e**) CH_2O/MnDV-GN, (**f**) H_2S/MnDV-GN, (**g**) HCN/MnDV-GN, (**h**) CH_2O/MnN_4-GN, (**i**) H_2S/ MnN_4-GN and (**j**) HCN/ MnN_4-GN. (spin up (yellow) and spin down (cyan) isosurface value: 0.005e $Å^{-3}$).

Author Contributions: Conceptualization, P.W. and H.W.; methodology, T.X. and G.Z.; software, T.X.; validation, J.J. and C.T.; formal analysis, C.H. and H.W.; investigation, T.X. and C.Z.; writing, T.X. and C.Z.; supervision, H.W. All authors have read and agreed to the published version of the manuscript.

Funding: This study was funded by the Transformation of Scientific and Technological Achievements Programs of Higher Education Institutions in Shanxi (No. 2020CG032), the Cultivation Plan of Young Scientific Researchers in Higher Education Institutions of Shanxi Province, and the Fund for Shanxi "1331 Project".

Data Availability Statement: All data generated or analysed during this study are included in this published article and its supplementary information files.

Acknowledgments: The authors would like to thank the Transformation of Scientific and Technological Achievements Programs and Higher Education Institutions of Shanxi Province to provide the funding support; and Haisun Wu for his technical assistance.

Conflicts of Interest: The authors declare no conflict of interest.

References

1. Faye, O.; Raj, A.; Mittal, V.; Beye, A.C. H_2S Adsorption on Graphene in the Presence of Sulfur: A Density Functional Theory Study. *Comp. Mater. Sci.* **2016**, *117*, 110–119. [CrossRef]
2. Ashori, E.; Nazari, F.; Illas, F. Adsorption of H_2S on Carbonaceous Materials of Different Dimensionality. *Int. J. Hydrog. Energy* **2014**, *39*, 6610–6619. [CrossRef]
3. Salthammer, T. Formaldehyde in the Ambient Atmosphere: From an Indoor Pollutant to an Outdoor Pollutant. *Angew. Chem. Int. Ed.* **2013**, *52*, 3320–3327. [CrossRef] [PubMed]
4. Noorizadeh, S.; Shakerzadeh, E. Formaldehyde Adsorption on Pristine, Al-doped and Mono-vacancy Defected Boron Nitride Nanosheets: A First Principles Study. *Comp. Mater. Sci.* **2012**, *56*, 122–130. [CrossRef]
5. Rastegar, S.F.; Peyghan, A.A.; Hadipour, N.L. Response of Si- and Al-Doped Graphenes toward HCN: A Computational Study. *Appl. Surf. Sci.* **2013**, *265*, 412–417. [CrossRef]
6. Peyghan, A.A.; Hadipour, N.L.; Bagheri, Z. Effects of Al Doping and Double-Antisite Defect on the Adsorption of HCN on a BC_2N Nanotube: Density Functional Theory Studies. *J. Phys. Chem. C* **2013**, *117*, 2427–2432. [CrossRef]

7. Wang, L.Z.; Mullen, K. Transparent, Conductive Graphene Electrodes for Dye-sensitized Solar Cells. *Nano Lett.* **2008**, *8*, 323–327. [CrossRef]
8. Tombros, C.Z.N.; Popinciuc, M.; Jonkman, H.T.; Wees, B.J.V. Electronic Spin Transport and Spin Precession in Single Graphene Layers at Room Temperature. *Nature* **2007**, *448*, 571–574. [CrossRef]
9. Schedin, F.; Geim, A.K.; Morozov, S.V.; Hill, E.W.; Blake, P.; Katsnelson, M.I.; Novoselov, K.S. Detection of Individual Gas Molecules Adsorbed on Graphene. *Nat. Mater.* **2007**, *6*, 652–655. [CrossRef]
10. Stankovich, S.; Dikin, D.A.; Dommett, G.H.; Kohlhaas, K.M.; Zimney, E.J.; Stach, E.A.; Piner, R.D.; Nguyen, S.T.; Ruoff, R.S. Graphene-Based Composite Materials. *Nature* **2006**, *442*, 282–286. [CrossRef]
11. Chhowalla, M.; Jena, D.; Zhang, H. Two-Dimensional Semiconductors for Transistors. *Nat. Rev. Mater.* **2016**, *1*, 16052. [CrossRef]
12. Novoselov, K.S.; Geim, A.K.; Morozov, S.V.; Jiang, D.; Zhang, Y.; Dubonos, S.V.; Grigorieva, I.V.; Firsov, A.A. Electric Field Effect in Atomically Thin Carbon Films. *Science* **2004**, *306*, 666–669. [CrossRef]
13. He, C.Z.; Wang, R.; Yang, H.Y.; Li, S.; Fu, L. The Growth Pattern of Pt_n (n = 1–6) Clusters on Pentagonal B_2C Monolayer Support: A Computational Study. *Appl. Surf. Sci.* **2020**, *507*, 145076. [CrossRef]
14. He, C.Z.; Wang, R.; Xiang, D.; Li, X.Y.; Fu, L.; Jian, Z.Y.; Huo, J.R.; Li, S. Charge-regulated CO_2 Capture Capacity of Metal Atom Embedded Graphyne: A First-Principles Study. *Appl. Surf. Sci.* **2020**, *509*, 145392. [CrossRef]
15. Wang, J.; He, C.Z.; Huo, J.R.; Fu, L.; Zhao, C.X. A Theoretical Evaluation of Possible N_2 Reduction Mechanism on Mo_2B_2. *Adv. Theory Simul.* **2021**, *4*, 2100003. [CrossRef]
16. Zhou, D.W.; Li, C.P.; Yin, F.R.; Tang, X.; Pu, C.Y.; He, C.Z. Two-dimensional 1T-PS_2 as a Promising Anode Material for Sodium-ion Batteries with Ultra-high Capacity, Low Average Voltage and Appropriate Mobility. *Chin. Chem. Lett.* **2020**, *31*, 2325–2329. [CrossRef]
17. Pu, C.Y.; Yu, J.H.; Fu, L.; Wang, J.; Yang, H.Y.; Zhou, D.W.; He, C.Z. Two-dimensional $MgSiP_2$ with anisotropic electronic properties and good performances for Na-ion batteries. *Chin. Chem. Lett.* **2021**, *32*, 1081–1085. [CrossRef]
18. Fu, X.; Yang, H.Y.; Fu, L.; He, C.Z.; Huo, J.R.; Guo, J.Y.; Li, L.M. Prediction of Semiconducting SiP_2 Monolayer with Negative Possion's Ratio, Ultrahigh Carrier Mobility and CO_2 Capture Ability. *Chin. Chem. Lett.* **2021**, *32*, 1089–1094. [CrossRef]
19. Fu, L.; Yan, L.B.; Lin, L.; Xie, K.; Zhu, L.H.; He, C.Z.; Zhang, Z.Y. Fe-embedded Au (111) Monolayer as An Electrocatalyst for N_2 Reduction Reaction: A First-principles Investigation. *J. Alloys Compd.* **2021**, *875*, 159907. [CrossRef]
20. Wang, R.; He, C.Z.; Chen, W.X.; Zhao, C.X.; Huo, J.R. Rich B Active Centers in Penta-B_2C as High-performance Photocatalyst for Nitrogen Reduction. *Chin. Chem. Lett.* **2021**, *32*, 3821–3824. [CrossRef]
21. Yang, H.Y.; He, C.Z.; Fu, L.; Huo, J.R.; Zhao, C.X.; Li, X.Y.; Song, Y. Capture and Separation of CO_2 on BC_3 Nanosheets: A DFT Study. *Chin. Chem. Lett.* **2021**, *32*, 3202–3206. [CrossRef]
22. Sun, R.S.; He, C.Z.; Fu, L.; Huo, J.R.; Zhao, C.X.; Li, X.Y.; Song, Y.; Wang, S.M. Defect Engineering for high-selection-performance of NO reduction to NH_3 over CeO_2(111) Surface: A DFT Study. *Chin. Chem. Lett.* **2022**, *33*, 527–532. [CrossRef]
23. Fu, L.; Wang, R.; Zhao, C.X.; Huo, J.R.; He, C.Z.; Kim, K.H.; Zhang, W. Construction of Cr-embedded Graphyne Electrocatalyst for Highly Selective Reduction of CO_2 to CH_4: A DFT Study. *Chem. Engin. J.* **2021**, *414*, 128857. [CrossRef]
24. Ma, D.W.; Wang, Q.G.; Yang, G.; He, C.Z.; Ma, B.Y.; Lu, Z.S. Graphyne as a Promising Substrate for the Noble-Metal Single-atom Catalysts. *Carbon* **2015**, *95*, 756–765. [CrossRef]
25. Deng, D.H.; Bao, X.H. A Graphene Composite Material with Single Cobalt Active Sites: A Highly Efficient Counter Electrode for Dye-Sensitized Solar Cells. *Angew. Chem. Int. Ed.* **2016**, *55*, 6708–6712.
26. Lu, Y.H.; Zhang, C.; Feng, Y.P. Metal-embedded Graphene: A Possible Catalyst with High Activity. *J. Phys. Chem. C* **2009**, *113*, 20156–20160. [CrossRef]
27. Gao, Z.; Li, A.; Liu, X.; Ma, C.; Li, X.; Yang, W.; Ding, X. Density Functional Study of the Adsorption of NO on Ni (n = 1, 2, 3 and 4) Clusters Doped Functionalized Graphene Support. *Appl. Surf. Sci.* **2019**, *481*, 940–950. [CrossRef]
28. Gao, Z.; Xu, S.; Li, L.; Yan, G.; Yang, W.; Wu, C.; Gates, I.D. On the Adsorption of Elemental Mercury on Single-atom TM (TM = V, Cr, Mn, Co) Decorated Graphene Substrates. *Appl. Surf. Sci.* **2020**, *516*, 146037. [CrossRef]
29. Shi, L.B.; Wang, Y.P.; Dong, H.K. First-Principle Study of Structural, Electronic, Vibrational and Magnetic Properties of HCN Adsorbed Graphene Doped With Cr, Mn and Fe. Appl. *Surf. Sci.* **2015**, *329*, 330–336. [CrossRef]
30. Sharma, S.; Verma, A.S.A. Theoretical Study of H_2S Adsorption on Graphene Doped with B, Al and Ga. *Phys. B* **2013**, *427*, 12–16. [CrossRef]
31. Gao, Z.; Yang, W.; Ding, X.; Lv, G.; Yan, W. Support Effects in Single Atom Iron Catalysts on Adsorption Characteristics of Toxic Gases (NO_2, NH_3, SO_3 and H_2S). *Appl. Surf. Sci.* **2018**, *436*, 585–595. [CrossRef]
32. Zhang, Y.H.; Han, L.F.; Xiao, Y.H.; Jia, D.Z.; Guo, Z.H.; Li, F. Understanding Dopant and Defect Effect on H_2S Sensing Performances of Graphene: A First-Principles Study. Comp. *Mater. Sci.* **2013**, *69*, 222–228. [CrossRef]
33. Zhang, H.P.; Luo, X.G.; Song, H.T.; Lin, X.Y.; Lu, X.; Tang, Y. DFT Study of Adsorption and Dissociation Behavior of H_2S on Fe-doped Graphene. *Appl. Surf. Sci.* **2014**, *317*, 511–516. [CrossRef]
34. Impeng, S.; Junkaew, A.; Maitarad, P.; Kungwan, N.; Zhang, D.; Shi, L.; Namuangruk, S. A MnN_4 Moiety Embedded Graphene as a Magnetic Gas Sensor for CO Detection: A First Principle Study. *Appl. Surf. Sci.* **2019**, *473*, 820–827. [CrossRef]
35. Chi, M.; Zhao, Y.P. Adsorption of Formaldehyde Molecule on the Intrinsic and Al-Doped Graphene: A First Principle Study. *Comp. Mater. Sci.* **2009**, *46*, 1085–1090. [CrossRef]

36. Robertson, A.W.; Montanari, B.; He, K.; Kim, J.; Allen, C.S.; Wu, Y.A.; Olivier, J.; Neethling, J.; Harrison, N.; Kirkland, A.I.; et al. Dynamics of Single Fe Atoms in Graphene Vacancies. *Nano Lett.* **2013**, *13*, 1468–1475. [CrossRef] [PubMed]
37. Lin, Y.C.; Teng, P.Y.; Yeh, C.H.; Koshino, M.; Chiu, P.W.; Suenaga, K. Structural and Chemical Dynamics of Pyridinic-Nitrogen Defects in Graphene. *Nano Lett.* **2015**, *15*, 7408–7413. [CrossRef]
38. Fujimoto, Y.; Saito, S. Formation, Stabilities, and Electronic Properties of Nitrogen Defects in Graphene. *Phys. Rev. B* **2011**, *84*, 245446. [CrossRef]
39. Liu, Z.Y.; Liu, K.K.; Chen, W.G.; Tang, Y.N. Structural, Electronic and Catalytic Performances of Single-Atom Fe Stabilized by Divacancy-Nitrogen-Doped Graphene. *RSC Adv.* **2017**, *7*, 7920–7928. [CrossRef]
40. Lu, Z.S.; He, C.Z.; Wang, T.X.; Yang, L.; Yang, Z.X.; Ma, D.W. Novel Catalytic Activity for Oxygen Reduction Reaction on MnN_4 Embedded Graphene: A Dispersion-Corrected Density Functional Theory Study. *Carbon* **2015**, *84*, 500–508. [CrossRef]
41. Banhart, J.K.F.; Krasheninnikov, A.V. Structural Defects in Graphene. *ACS Nano* **2011**, *5*, 26–41. [CrossRef] [PubMed]
42. Dewapriya, M.A.N. Effects of Free Edges and Vacancy Defects on the Mechanical Properties of Graphene. *Nanotechnology* **2014**, *12*, 908–912.
43. Kresse, G.; Furthmuller, J.J.B. Efficient Iterative Schemes for Ab Initio Total-Energy Calculations Using a Plane-Wave Basis Set. *Phys. Rev. B* **1996**, *54*, 11169. [CrossRef]
44. Perdew, J.P.; Burke, K.; Ernzerhof, M. Generalized Gradient Approximation Made Simple. *Phys. Rev. Lett.* **1996**, *77*, 3865–3868. [CrossRef] [PubMed]
45. Kresse, G.; Joubert, D. From Ultrasoft Pseudopotentials to the Projector Augmented-Wave Method. *Phys. Rev. B* **1999**, *59*, 1758–1775. [CrossRef]
46. Xie, T.; Wang, P.; Tian, C.; Zhao, G.; Jia, J.; He, C.; Zhao, C.; Wu, H.; Michel, C. The Investigation of Adsorption Behavior of Gas Molecules on FeN3-Doped Graphene. *J. Sens.* **2022**, *2022*, 9306741. [CrossRef]
47. Xie, T.; Wang, P.; Tian, C.; Zhao, G.; Jia, J.; Zhao, C.; Wu, H. The Adsorption Behavior of Gas Molecules on Co/N Co-Doped Graphene. *Molecules* **2021**, *26*, 7700. [CrossRef]
48. Grimme, S.; Antony, J.; Ehrlich, S.; Krieg, H. A consistent and accurate ab initio parametrization of density functional dispersion correction (DFT-D) for the 94 elements H-Pu. *J. Chem. Phys.* **2010**, *132*, 154104. [CrossRef]
49. Santos, E.J.G.; Ayuela, A.; Sanchez-Portal, D. First-principles Study of Substitutional Metal Impurities in Graphene: Structural, Electronic and Magnetic Properties. *New J. Phys.* **2010**, *12*, 053012. [CrossRef]
50. Kattel, S.; Atanassov, P.; Kiefer, B. Stability, Electronic and Magnetic Properties of In-plane Defects in Graphene: A First-Principles Study. *J. Phys. Chem. C* **2012**, *116*, 8161–8166. [CrossRef]
51. Sun, S.; Zhang, G.; Gauquelin, N.; Chen, N. Single-Atom Catalysis Using Pt/Graphene Achieved through Atomic Layer Deposition. *Sci. Rep.* **2013**, *3*, 1775. [CrossRef]
52. Momma, K.; Izumi, F. Three-Dimensional Visualization of Crystal, Volumetric and Morphology Data. *J. Appl. Crystallogr.* **2011**, *44*, 1272–1276. [CrossRef]
53. Dronskowski, R. Crystal Orbital Hamilton Populations (COHP), Energy-Resolved Visualization of Chemical Bonding in Solids Based on Density-Functional Calculations. *J. Phys. Chem.* **1993**, *97*, 8617–8624. [CrossRef]
54. Deringer, V.L.; Tchougreeff, A.L.; Dronskowski, R. Crystal Orbital Hamilton Population (COHP) Analysis as Projected from Plane-Wave Basis Sets. *J. Phys. Chem. A* **2011**, *115*, 5461–5466. [CrossRef] [PubMed]
55. Maintz, S.; Deringer, V.L.; Tchougreeff, A.L.; Dronskowski, R. LOBSTER: A Tool to Extract Chemical Bonding from Plane-Wave Based DFT. *J. Comput. Chem.* **2016**, *37*, 1030–1035. [CrossRef] [PubMed]
56. Henkelman, G.; Arnaldsson, A.; Jonsson, H. A Fast and Robust Algorithm for Bader Decomposition of Charge Density. *Comput. Mater. Sci.* **2006**, *36*, 354–360. [CrossRef]
57. Krasheninnikov, A.V.; Lehtinen, P.O.; Foster, A.S.; Pyykko, P.; Nieminen, R.M. Embedding Transition-Metal Atoms in Graphene: Structure, Bonding, and Magnetism. *Phys. Rev. Lett.* **2009**, *102*, 126807. [CrossRef]
58. Woolley, J.C. Introduction to Solid State Physics: C. Kittel: 2nd Edition. Chapman and Hall, 1956. 617 pp., 96s. *J. Mech. Phys. Solids* **1957**, *6*, 83. [CrossRef]
59. Feng, C.; Yang, D.G.; Zhang, G.Q. First-Principles Investigation of the Adsorption Behaviors of CH_2O on BN, AlN, GaN, InN, BP and P Monolayers. *Materials* **2019**, *12*, 676. [CrossRef]
60. Gao, X.; Wang, J.X.; Xu, L.N.; Zeng, W. Performance of Intrinsic and Modified Graphene for the Adsorption of H_2S and CH_4: A DFT Study. *Nanomaterials* **2020**, *10*, 299. [CrossRef]
61. Tang, Y.; Chen, W.; Li, C.; Pan, L.; Dai, X.; Ma, D. Adsorption Behavior of Co Anchored on Graphene Sheets toward NO, SO_2, NH_3, CO and HCN Molecules. *Appl. Surf. Sci.* **2015**, *342*, 191–199. [CrossRef]
62. Fukui, K. Role of Frontier Orbitals in Chemical Reactions. *Science* **1982**, *218*, 747–754. [CrossRef] [PubMed]
63. Huang, B.; Xiao, L.; Lu, J.; Zhuang, L. Spatially Resolved Quantification of the Surface Reactivity of Solid Catalysts. *Angew. Chem. Int. Ed.* **2016**, *55*, 6239–6243. [CrossRef] [PubMed]
64. Yang, W.; Gao, Z.; Ding, X.; Lv, G.; Yan, W. The Adsorption Characteristics of Mercury Species on Single Atom Iron Catalysts with Different Graphene-Based Substrates. *Appl. Surf. Sci.* **2018**, *455*, 940–951. [CrossRef]